KFUPM
Journal of Undergraduate Research International

Diamond Open Access

Article
Computer Science

Cutting Parameter, Cutting Force, and Tool Vibration Correlations for Predicting Surface Roughness During 42CrMo4+QT Turning

Farah Mohammed Fallata, Muhammad Fadhlan Afif*, and Ahmed Aly Diaa Sarhan*

Cite https://doi.org/10.64589/juri/214967

Submitted: October 17, 2025 **Revised:** October 28, 2025 **Accepted:** December 1, 2025

ABSTRACT

This study processed and analyzed data describing tool holder force and acceleration during the high-accuracy turning of high-strength alloy steel (42CrMo4+QT) workpieces under different cutting conditions to identify the features most strongly correlated with surface quality, which was defined as the machined surface roughness *Ra* in this study. The time-domain force signals were filtered to remove noise before extracting their average, maximum, minimum, and standard deviation features, and the frequency-domain acceleration signals were filtered and analyzed to obtain spectral features reflecting dynamic vibrations during cutting. The correlations between the extracted features and *Ra* were evaluated using the Pearson and Spearman rank coefficients; the results indicated that the tool corner radius, feed rate, and depth of cut exerted critical influences on *Ra*. Furthermore, the combined average cutting force features in all directions exhibited better correlation with *Ra* the acceleration features. Indeed, the corner radius, feed rate, depth of cut, and combined average multidirectional cutting force predicted *Ra* with adequate accuracy and significance. It can serve as reliable indicators for predicting workpiece surface quality as a result. This conclusion can inform the development of efficient methods for real-time monitoring and quality control during the turning of high-strength alloy steel-workpieces.

Keywords: machining, turning, cutting force, vibration, surface roughness

1. INTRODUCTION

Surface quality is a critical consideration during workpiece turning operations, particularly when machining high-strength alloy steel parts commonly used in the aerospace, automotive, energy, and defense industries that must provide high dimensional accuracy, functional reliability, and fatigue resistance. Notably, the surface roughness of a part has been found to influence its wear, fatigue life, and tribological function [1]. This has motivated investigations into which manufacturing parameters exert the most influence on surface roughness.

Although the performance of high-strength steel materials has long been considered sufficient, the process used to machine parts from such materials must be improved to ensure that the full benefits of the material properties are realized. This is especially true when conducting high accuracy turning operations using smaller work engagement than applied in general turning operations. Critically, the optimal cutting parameters must be employed during the turning process to ensure efficient manufacturing and satisfy quality requirements. However, the nonlinear mechanical behaviors, work hardening, and elevated cutting parameters associated with machining high-strength alloys can affect the wear and surface finish of the resulting parts. These conditions can be characterized by process parameters such as cutting force, vibration, and heat [2]. Therefore, determination of which parameters should be used to characterize turning operations is a critical subject of research, particularly for processes employing small cutting depths and high-strength alloys with relatively low surface roughness ranges.

This study accordingly analyzed the raw signal dataset provided by Diaz et al. [3] to investigate the effects of cutting parameters, forces, and vibrations on surface quality because the authors of this dataset have not considered vibration data in their published research [4,5]. The Pearson and Spearman rank correlation analysis were used to identify the critical features in this study as they have been widely applied to similar numerical datasets [6,7]. The results of this study are expected to provide a basis for the selection of critical features when developing machine learning models to predict surface quality. Indeed, appropriate feature selection can reduce the complexity of a prediction model without sacrificing its performance while simplifying data management and storage requirements.

This remainder of this paper is organized as follows: Section 2 describes the methods employed by Diaz et al. [3] to collect the data used in this study; Section 3 details the methodology used for signal processing and feature extraction; Section 4 presents the applied analysis methods and resulting correlations between the surface roughness and cutting parameter, force, and vibration features; finally, Section 5 summarizes the conclusions of this study and their contributions to future research.

Table 1. *Chemical composition of 42CrMo4 steel*[8]

C	Mn	Si	P	S	Cu	Cr	Ni	Al	Mo	V	Ti	Sn
0.42	0.64	0.21	0.013	0.009	0.02	1.04	0.06	0.026	0.185	0.006	0.0013	0.003

2. DATA COLLECTION

This section describes the methods employed by Diaz et al.[3] to collect the data used in this study. Although this information does not represent the present work, it provides critical details describing how the data were obtained and informs the signal processing methods applied in this study.

2.1. Material Properties. The workpieces were made of 42CrMo4+QT steel, which possesses high impact and fatigue resistance[3,8]. The chemical composition and mechanical properties of this material are listed in Table 1[8] and Table 2[4], respectively.

2.2. Experimental Scheme. The turning process (cutting) parameters defined in Figure 1 comprise the insert radius (r), cutting depth (a), feed (f), and cutting speed (v), which was determined based on the spindle rotational speed (n) as follows:

$$v = n\pi D \tag{1}$$

where D is the workpiece diameter.

The forces and vibrations acting on the tool holder were measured using sensors to obtain the cutting forces in all three directions (Fx, Fy, and Fz) and tool vibrations in the x- and y-directions (as acceleration ax and ay), as shown in Figure 1.

2.3. Machine and Equipment. The specifications of the computer numerical control (CNC) lathe used by Diaz et al.[3] for the turning operations are described in Table 3, and the specifications of the cutting inserts used to perform the turning operations are listed in Table 4[3,9,10]. A confocal microscope was used with the settings detailed in Table 5[3] to measure the surface profile after each workpiece was machined and thereby determine its surface roughness Ra, as depicted in Figure 1. The turning process parameters (cutting force and vibration signals) were recorded using the data acquisition system specified in Table 6[3]. Finally, the LabView software was used to collect the measured cutting parameter data from the data acquisition system.

2.4. Design of Experiment. Diaz et al.[3] varied the cutting parameters applied during the turning process using the combinations shown in Table 7. The final dataset contained 68 records comprising 34 combinations of f, v, and a values with 2 different $r$values.

3. DATASET SIGNAL PROCESSING

3.1. Cutting Force Signals. Savitzky–Golay filtering[11,12] was performed to cancel out the noise present in the raw signals. A typical result of applying this filtering process is shown in Figure 2, indicating that the third filtering pass adequately eliminated the influence of noise.

The raw signals in each record comprised several components corresponding to different steps in the turning process, as shown in Figure 3. The correlation analysis conducted in this study focused on the data collected during the finishing operations by applying time-interval windows to isolate the desired raw signal from each operation. This segmentation strategy excluded the first- and last-contact signals of each operation from the analysis because sudden peaks that may produce outlier data are often observed in these regions.

The mean (Avg), maximum (Max), minimum (Min), and standard deviation (Std) metrics of the Fx, Fy, and Fz data in each window were extracted, and the average value of each metric from all four windows was considered to represent each feature that record. In addition, the combined average forces in all three directions, defined as $AvgFc$, was determined follows:

$$AvgFc = \sqrt{AvgFx^2 + AvgFy^2 + AvgFy^2} \tag{2}$$

3.2. Vibration Signals. For the same time interval (window), the acceleration signal is segmented and passed to the Fast-Fourier Transform (FFT) and the subsequent vibration analysis[13,14]. These signals were decomposed into multiple components with frequencies ranging from zero to half of the sampling frequency. The FFT output consists of complex values; the absolute value (magnitude) of these complex numbers represents the amplitude of the signal at each specific frequency. This allows for the identification of dominant frequencies within the tool holder's vibration signal.

Figure 4 shows that the dominant frequency was identified at 3124 and 9375 Hz, representing the natural frequencies of the cutting tool which are critical factors in exciting chatter and thereby increase surface roughness. The frequencies with the highest amplitudes in the x- and y-directions—9375 Hz for both in this case—were defined as ωnx and ωny and passed to the dataset for correlation analysis.

The values of the different features extracted by the signal processing methods detailed in this section are listed in Table 8; the Ra values were obtained directly from the dataset[3].

Table 2. *Mechanical properties of 42CrMo4 steel*[4]

Mechanical properties	Value
Yield stress (MPa)	Stainless-steel
Tensile stress (MPa)	1097
Hardness (HV10)	310–370
Impact toughness (KV)	83.5 at 20 °C

Table 3. *Specifications of the CNC lathe used in the experiments*[3]

Model	JATOR TAJ-42
Machine software	Fagor 8055 T
Main speed engine power	11/15 kW
Maximum spindle speed	3000 rpm
Spindle nose	DIN 55,026 (A5)

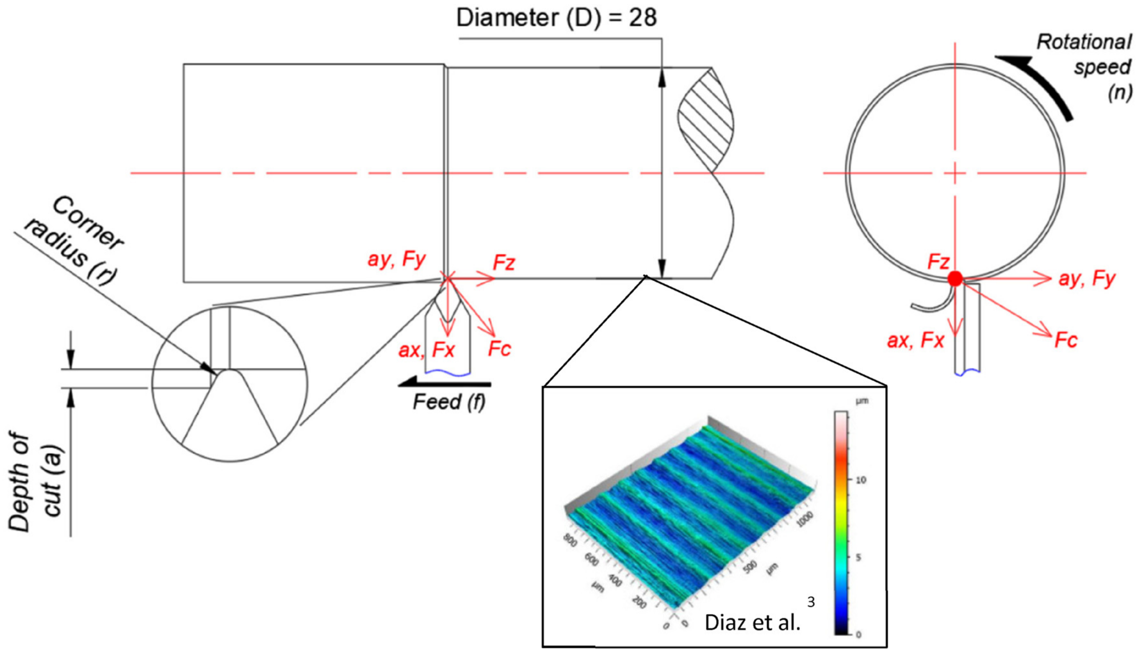

Figure 1. Cutting parameters, cutting forces, and surface roughness profile associated with the applied turning process

Table 4. *Specifications of the cutting inserts used in the experiments*[3,9,10]

Insert manufacturer	Sandvik Coromant	Sandvik Coromant
Model	**DCMX 11 T3 04-WF 4325**	**DCMX 11 T3 08-WF 4425**
Tip radius (mm)	0.4	0.8
Main cutting-edge angle (°)	93	93
Recommended *a* (mm)	1	1.5
Recommended *v* (m/min)	345–475	305–420
Recommended *f* (mm/rev)	0.07–0.30	0.12–0.4

4. FEATURE CORRELATION ANALYSIS

A correlation analysis was performed to investigate the influences of the obtained features on *Ra*. First, the Pearson correlation coefficient (Rp_{xy})[6,7] for each pair of features was obtained as follows:

$$Rp_{xy} = \frac{\sum_{i=1}^{m} (x_i - \bar{x}) (y_i - \bar{y})}{\sqrt{\sum_{i=1}^{m} (x_i - \bar{x})^2}\sqrt{\sum_{i=1}^{m} (y_i - \bar{y})^2}} \tag{3}$$

where x_i is the value of i-th record for feature x, $\bar{x}$ is the average of all feature x values, y_i is the value of i-th record for feature y, $\bar{y}$ is the average of all feature y values, and m is the total number of features.

The Pearson correlation coefficient ranges from −1 to 1; a positive coefficient indicates that an increase in feature x results

Table 5. *Leica DCM3 confocal microscope settings*[3]

Applied standard	UNE-EN ISO 21920-3
Objective magnification	10x
Measured parameter	Ra
Selected cut-off (λ_c) (mm)	0.80
Evaluation length (mm)	5.60
Evaluation width (mm)	0.95
Evaluation area (mm^2)	5.32

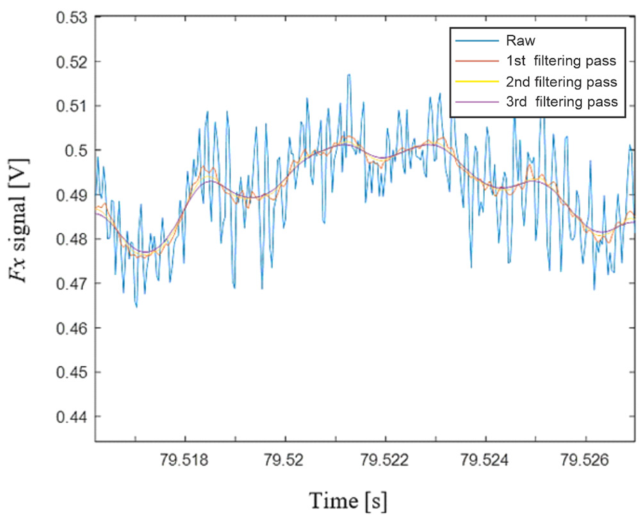

Figure 2. Results of Savitzky–Golay filtering on an example cutting force signal

Table 6. *Data acquisition system details* [3]

Procurement module		NI 9269/NI 9234	
Acquisition chassis		NI cDAQ-9174	
Parameter	**Register units**	**SI units**	**Conversion**
Acceleration X, Y	Gravity (g)	m/s^2	$9.8\ (m/s^2)/g$
Force X	V	N	100 N/V
Force Y	V	N	100 N/V
Force Z	V	N	100 N/V

in an increase in feature y, whereas a negative coefficient indicates that an increase in feature x results in a decrease in feature y, and the magnitude of the coefficient reflects the strength of the correlation. Note that the Pearson correlation assumes that the relationship between the two considered features is linear and reflects only the closeness, not the slope of that relationship.

Therefore, the Spearman rank correlation coefficient (Rs_{xy}) [15] was also evaluated to determine whether a nonlinear (monotonic) relationship existed between features. Notably, Spearman rank correlation can compare abnormally distributed or outlier features. First, the numerical feature data were ranked (sorted) and the possibility of ties between records was considered and addressed [15], then the Spearman rank correlation was determined as follows:

$$Rs_{xy} = \frac{\sum_{i=1}^{m}\left(Rx_i - \overline{Rx}\right)\left(Ry_i - \overline{Ry}\right)}{\sqrt{\sum_{i=1}^{m}\left(Rx_i - \overline{Rx}\right)^2}\sqrt{\sum_{i=1}^{m}\left(Ry_i - \overline{Ry}\right)^2}} \tag{4}$$

where Rx_i and Ry_i are the values of i-th ranked features x and y, respectively, and $\overline{Rx}$ and $\overline{Ry}$ are the mean ranks for all records of features x and y, respectively.

The Spearman rank correlation coefficient varies within the same range as the Pearson correlation coefficient, and its sign indicates the same relationships. Evaluating the correlations between features using both the Pearson and Spearman rank coefficients can provide insight into the relationships between features, as shown in the example in Figure 5. The features that have low Pearson and Spearman rank coefficients (third quadrant) should be flagged as features that might cause noise on the prediction models. However, if at least one coefficient gives high value, the relationship between the two features can be estimated as shown.

The Pearson and Spearman rank correlation coefficients between all features were calculated using Equations (3) and (4), respectively, and are shown in the heat maps in Figure 6 and 7, respectively. The diagonal values in both figures are all equal to 1, confirming perfect correlation between identical features. Note that these heat maps show not only the correlations between the features and Ra, but also those among the features themselves.

Therefore, the heat map values in the row and column corresponding to correlations with Ra were used to generate the

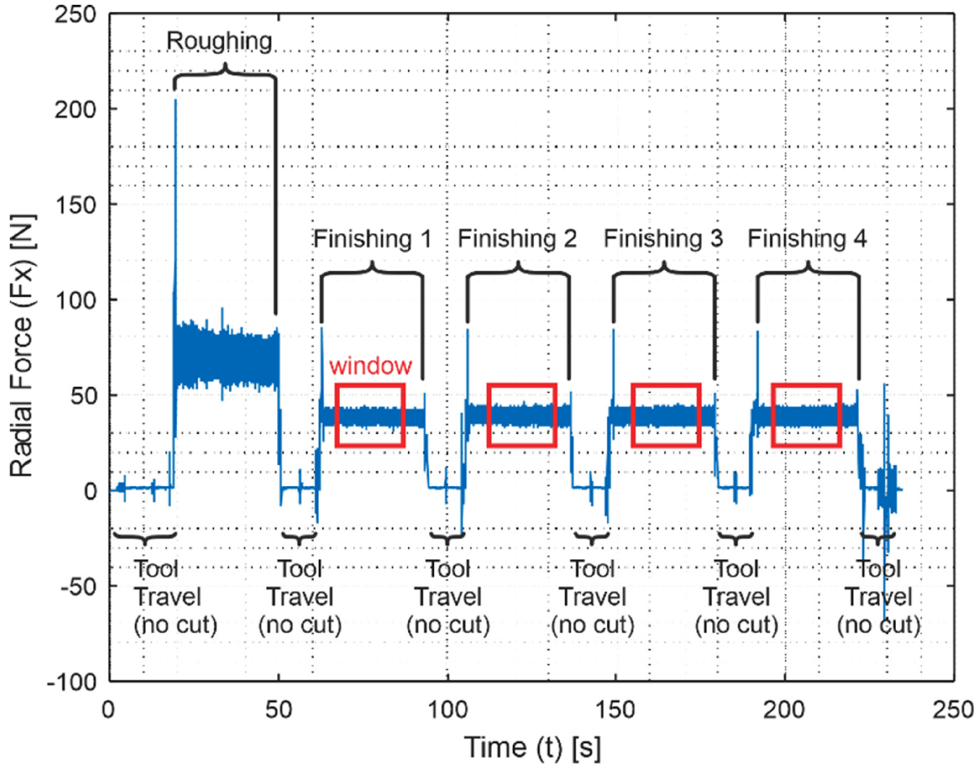

Figure 3. Signal segmentation strategy

Table 7. *Cutting parameters applied during the turning experiments*[3]

Parameter		Units	Values				
Feed rate	f	mm/rev	0.05	0.1	0.15	0.2	0.25
Cutting speed	v	m/min	76	107	138	169	200
Depth of cut	a	mm	0.05	0.1	0.15	0.2	0.25
Insert radius	r	mm	0.4	0.8	-	-	-

Run	r	a	v	f	Run	r	a	v	f
1	0.4	0.05	138	0.15	**35**	0.8	0.05	138	0.15
2	0.4	0.05	138	0.15	**36**	0.8	0.05	138	0.15
3	0.4	0.10	107	0.10	**37**	0.8	0.10	107	0.10
4	0.4	0.10	107	0.10	**38**	0.8	0.10	107	0.10
5	0.4	0.10	107	0.20	**39**	0.8	0.10	107	0.20
6	0.4	0.10	107	0.20	**40**	0.8	0.10	107	0.20
7	0.4	0.10	169	0.20	**41**	0.8	0.10	169	0.20
8	0.4	0.10	169	0.20	**42**	0.8	0.10	169	0.20
9	0.4	0.10	169	0.10	**43**	0.8	0.10	169	0.10
10	0.4	0.10	169	0.10	**44**	0.8	0.10	169	0.10
11	0.4	0.15	76	0.15	**45**	0.8	0.15	76	0.15
12	0.4	0.15	76	0.15	**46**	0.8	0.15	76	0.15
13	0.4	0.15	138	0.05	**47**	0.8	0.15	138	0.05
14	0.4	0.15	138	0.05	**48**	0.8	0.15	138	0.05
15	0.4	0.15	138	0.15	**49**	0.8	0.15	138	0.15
16	0.4	0.15	138	0.15	**50**	0.8	0.15	138	0.15
17	0.4	0.15	138	0.15	**51**	0.8	0.15	138	0.15
18	0.4	0.15	138	0.15	**52**	0.8	0.15	138	0.15
19	0.4	0.15	138	0.15	**53**	0.8	0.15	138	0.15
20	0.4	0.15	138	0.15	**54**	0.8	0.15	138	0.15
21	0.4	0.15	138	0.25	**55**	0.8	0.15	138	0.25
22	0.4	0.15	138	0.25	**56**	0.8	0.15	138	0.25
23	0.4	0.15	200	0.15	**57**	0.8	0.15	200	0.15
24	0.4	0.15	200	0.15	**58**	0.8	0.15	200	0.15
25	0.4	0.20	107	0.10	**59**	0.8	0.20	107	0.10
26	0.4	0.20	107	0.10	**60**	0.8	0.20	107	0.10
27	0.4	0.20	107	0.20	**61**	0.8	0.20	107	0.20
28	0.4	0.20	107	0.20	**62**	0.8	0.20	107	0.20
29	0.4	0.20	169	0.20	**63**	0.8	0.20	169	0.20
30	0.4	0.20	169	0.20	**64**	0.8	0.20	169	0.20
31	0.4	0.20	169	0.10	**65**	0.8	0.20	169	0.10
32	0.4	0.20	169	0.10	**66**	0.8	0.20	169	0.10
33	0.4	0.25	138	0.15	**67**	0.8	0.25	138	0.15
34	0.4	0.25	138	0.15	**68**	0.8	0.25	138	0.15

bar plot shown in Figure 8(a). The cutting force features clearly exhibited greater correlations with *Ra* than the vibration features. As a result, *AvgFc* can be used as the sole feature to differentiate and characterize the effects of various process parameters on *Ra* in the considered dataset. A bar plot showing the correlations between all features and *AvgFc* is accordingly provided in Figure 8(b). This result agrees with the conclusions of many previous studies that cutting forces can be used to characterize surface roughness[17–20].

In terms of the correlations between the key features and *Ra*, f clearly exerted the most influence on *Ra*, with Pearson and Spearman rank correlation coefficients of 0.71 and 0.68, respectively, followed by r, with coefficients of -0.41 and -0.44, respectively. Furthermore, most of the Pearson and Spearman rank correlation coefficients for the features were nearly identical, except for those corresponding to *StdFx, StdFy,* and *StdFz*. Together, these results suggest that the relationship between f and *Ra* is likely linear, whereas the relationships between the other features and *Ra* are nonlinear, complex, or reflect no correlation at all.

Interestingly, nearly all features, including *AvgFc*, were positively correlated with *Ra*, whereas $r, a,$and$v$ were negatively (although weakly) correlated with *Ra*. The reasons for these correlations can be observed in the empirical equations for estimating *Ra*, given by

$$Ra = \frac{0.0032f^2}{r} \tag{5}$$

and *Fc*, given by

$$Fc = k_c A \tag{6}$$

Table 8. *Features extracted by signal processing and analysis*

Run	*r*	*a*	*v*	*f*	*AvgFx*	*MaxFx*	*MinFx*	*StdFx*	*AvgFy*	*MaxFy*	*MinFy*	*StdFy*	*AvgFz*	*MaxFz*	*MinFz*	*StdFz*	*AvgFc*	*ωnx*	*ωny*	*Ra*
1	0.4	0.05	138	0.15	41.09	48.37	33.80	1.37	62.13	71.28	54.60	3.16	-9.29	-0.27	-16.63	3.93	75.06	8759	9375	0.858
2	0.4	0.05	138	0.15	40.84	46.79	34.20	1.19	54.10	60.18	49.97	0.94	-0.37	3.34	-4.52	0.90	67.79	8820	3125	1.078
3	0.4	0.1	107	0.1	39.05	46.50	32.82	1.34	43.55	47.77	39.23	0.91	-5.96	-1.52	-10.11	1.26	58.80	9375	9375	0.409
4	0.4	0.1	107	0.1	44.91	52.77	38.39	1.57	63.82	60.22	59.28	0.91	2.23	6.25	-1.85	1.22	78.07	8758	9375	0.558
5	0.4	0.1	107	0.2	51.70	108.37	-3.18	23.49	76.29	148.84	11.33	29.23	-11.48	20.10	-43.67	9.77	92.87	8809	9375	1.133
6	0.4	0.1	107	0.2	63.63	70.58	57.05	1.51	92.77	97.24	88.63	1.00	13.27	18.51	8.23	1.50	113.28	8809	9375	1.185
7	0.4	0.1	169	0.2	67.22	73.12	60.94	1.37	87.50	92.16	83.28	1.13	13.66	17.89	9.39	1.07	111.18	8720	3125	1.156
8	0.4	0.1	169	0.2	66.44	73.78	60.50	1.44	92.51	98.46	86.94	1.56	3.14	8.17	-2.25	1.81	113.94	8770	3125	1.140
9	0.4	0.1	169	0.1	49.49	59.04	43.14	1.68	59.81	66.25	54.16	1.62	3.19	7.74	-1.01	1.41	77.69	8723	9375	0.640
10	0.4	0.1	169	0.1	49.34	55.33	43.85	1.37	62.26	66.95	57.66	1.32	0.07	4.93	-4.25	1.56	79.44	9375	9375	0.561
11	0.4	0.15	76	0.15	61.69	70.96	52.39	1.93	97.96	103.86	92.30	1.46	-29.28	-18.98	-38.67	3.49	119.41	3125	3125	0.759
12	0.4	0.15	76	0.15	65.17	94.17	29.72	3.60	105.29	128.53	90.90	4.02	-31.50	-18.11	-43.99	2.41	127.77	3125	3125	0.806
13	0.4	0.15	138	0.05	37.21	54.37	22.95	2.12	38.43	49.83	31.77	2.07	35.68	51.72	16.35	7.72	64.29	3125	9375	0.306
14	0.4	0.15	138	0.05	63.88	83.64	44.55	3.34	171.72	188.87	158.84	3.45	59.91	78.82	46.75	3.91	192.76	9375	9375	0.657
15	0.4	0.15	138	0.15	58.71	65.46	52.32	1.43	91.16	96.03	85.98	1.13	-32.37	-25.75	-39.21	2.51	113.16	3125	9375	0.796
16	0.4	0.15	138	0.15	51.18	147.87	-7.28	31.68	120.23	346.49	-9.80	117.57	3.42	122.24	-62.01	59.57	130.72	9375	9375	0.849
17	0.4	0.15	138	0.15	65.63	73.24	59.50	1.44	95.03	99.79	90.90	1.01	-3.68	3.12	-10.90	2.79	115.55	9375	9375	0.675
18	0.4	0.15	138	0.15	63.68	70.57	57.57	1.42	90.90	96.58	86.12	1.17	-33.96	-26.22	-40.67	2.76	116.07	3125	9375	0.690
19	0.4	0.15	138	0.15	63.71	74.91	48.27	1.65	94.61	103.15	89.15	1.33	-34.99	-25.20	-44.66	4.20	119.31	9375	9375	0.888
20	0.4	0.15	138	0.15	56.98	63.96	50.27	1.52	74.21	79.09	69.54	1.06	13.31	19.92	6.75	2.46	94.51	9375	9375	0.870
21	0.4	0.15	138	0.25	83.31	95.09	72.27	2.12	129.99	142.76	123.11	1.97	-9.09	-1.26	-16.29	2.48	154.66	3125	9375	1.623
22	0.4	0.15	138	0.25	80.92	90.75	70.95	1.98	127.29	133.22	121.72	1.51	-9.01	-1.59	-16.26	2.50	151.10	3125	3125	1.682
23	0.4	0.15	200	0.15	73.31	81.41	65.47	1.85	94.08	100.61	86.99	1.66	-2.26	6.98	-11.00	3.91	119.29	3125	3125	0.587
24	0.4	0.15	200	0.15	73.31	82.14	63.39	1.84	96.82	104.82	89.30	1.80	-3.19	7.17	-13.11	4.23	121.49	9375	9375	0.596
25	0.4	0.2	107	0.1	53.74	62.21	46.11	1.75	90.43	97.05	83.74	1.53	-22.54	-9.76	-35.70	6.01	107.58	9375	9375	0.478
26	0.4	0.2	107	0.1	52.74	61.30	43.32	1.80	89.21	96.15	83.68	1.49	-21.21	-10.44	-31.07	4.45	105.78	3125	3125	0.574
27	0.4	0.2	107	0.2	86.94	98.85	71.76	2.53	120.73	127.90	113.22	1.85	-45.96	-31.12	-60.84	6.34	155.71	9375	9375	1.002
28	0.4	0.2	107	0.2	76.86	92.47	61.94	2.58	112.03	119.04	105.06	2.10	-28.67	-19.26	-38.84	3.79	138.85	9375	9375	1.074
29	0.4	0.2	169	0.2	92.08	104.52	78.65	2.91	125.64	133.40	117.50	2.18	18.94	30.00	7.23	3.89	156.92	3125	3125	1.111
30	0.4	0.2	169	0.2	87.29	97.80	75.56	2.42	118.32	125.01	111.60	1.65	10.89	22.89	-1.41	4.73	147.44	3125	3125	1.091
31	0.4	0.2	169	0.1	57.59	67.44	50.39	1.88	88.38	95.99	81.93	1.87	-19.57	-9.53	-28.89	3.85	107.29	3125	3125	0.432
32	0.4	0.2	169	0.1	58.44	67.98	50.69	1.93	89.01	96.43	82.82	1.78	16.21	28.04	4.79	5.22	107.71	9375	9375	0.460
33	0.4	0.25	138	0.15	69.60	79.22	60.12	1.98	109.35	114.92	102.75	1.34	-28.30	-16.64	-39.89	4.86	132.67	3125	3125	0.735
34	0.4	0.25	138	0.15	74.61	84.13	64.62	2.02	128.73	134.83	121.81	1.55	-33.15	-16.58	-49.74	7.56	152.43	8770	9375	0.783
35	0.8	0.05	138	0.15	37.93	48.45	30.25	1.45	60.89	65.90	56.58	1.03	-27.03	-23.48	-30.44	1.07	76.66	3125	3125	0.800
36	0.8	0.05	138	0.15	36.83	36.83	27.90	2.05	57.01	57.01	57.01	1.59	-35.04	-28.89	-38.63	0.86	76.39	3125	3125	1.069
37	0.8	0.1	107	0.1	32.50	44.55	22.37	1.73	44.49	51.23	31.06	1.58	-42.25	-1.92	-50.33	4.00	69.43	9375	9375	0.477
38	0.8	0.1	107	0.1	37.66	49.11	27.67	2.17	65.14	72.42	59.87	1.58	-42.77	-35.41	-49.87	3.00	86.55	9375	9375	0.551
39	0.8	0.1	107	0.2	52.20	61.96	43.69	1.74	73.44	77.71	69.23	0.98	-31.16	-25.21	-36.92	2.03	95.34	9375	9375	0.735
40	0.8	0.1	107	0.2	59.03	68.67	48.58	2.03	93.41	100.11	87.86	1.27	-27.99	18.34	-18.34	4.04	113.98	9375	9375	0.777
41	0.8	0.1	169	0.2	62.14	70.49	54.20	1.76	83.46	90.25	78.15	1.62	-30.00	-26.34	-33.56	0.96	108.29	9375	9375	0.730

(Continued)

Table 8. *Continued*

Run	*r*	*a*	*v*	*f*	*AvgFx*	*MaxFx*	*MinFx*	*StdFx*	*AvgFy*	*MaxFy*	*MinFy*	*StdFy*	*AvgFz*	*MaxFz*	*MinFz*	*StdFz*	*AvgFc*	*ωnx*	*ωny*	*Ra*
42	0.8	0.1	169	0.2	62.58	69.53	56.20	1.66	86.43	92.21	81.37	1.60	4.70	10.81	-0.99	2.02	106.81	3125	3125	0.727
43	0.8	0.1	169	0.1	43.02	51.41	37.59	1.47	65.52	72.28	60.84	1.25	18.72	-12.24	-25.39	2.64	80.58	3125	3125	0.544
44	0.8	0.1	169	0.1	42.98	53.44	36.99	1.68	64.04	71.05	58.90	1.38	-16.48	-10.11	-22.65	2.54	78.86	3125	3125	0.468
45	0.8	0.15	76	0.15	50.89	63.73	41.21	2.03	77.92	86.18	70.68	2.22	-47.64	-35.96	-58.82	5.06	104.55	9375	9375	3.235
46	0.8	0.15	76	0.15	57.91	69.28	44.37	2.18	100.64	108.43	92.94	1.91	-46.69	-33.65	-58.50	5.33	125.14	3125	3125	0.624
47	0.8	0.15	138	0.05	39.77	54.47	31.70	2.62	62.10	71.59	56.15	2.02	-37.94	-28.54	-46.71	3.93	82.93	3125	3125	0.307
48	0.8	0.15	138	0.05	44.13	67.65	24.80	3.49	65.77	82.31	58.15	2.22	-37.38	-23.87	-48.52	4.36	87.59	3125	3125	0.275
49	0.8	0.15	138	0.15	62.25	74.70	52.81	1.82	95.63	107.55	89.61	1.81	-42.18	-32.16	-53.09	4.02	121.65	9375	9375	0.488
50	0.8	0.15	138	0.15	64.79	89.57	37.63	3.10	102.95	115.56	91.21	2.79	-12.47	1.08	-26.37	4.95	122.28	3125	3125	0.555
51	0.8	0.15	138	0.15	63.14	70.31	55.73	1.61	97.41	103.36	93.10	1.12	-14.27	-2.53	-25.31	5.46	116.96	3125	3125	0.406
52	0.8	0.15	138	0.15	61.60	70.53	53.82	1.60	96.76	102.02	91.54	1.24	-13.84	-1.89	-25.71	5.67	115.53	3125	3125	0.410
53	0.8	0.15	138	0.15	60.23	67.28	53.60	1.48	94.19	98.73	89.64	1.06	-12.23	-1.49	-23.16	4.83	112.47	9375	9375	0.475
54	0.8	0.15	138	0.15	62.93	129.83	-15.83	4.28	112.73	164.98	83.24	10.70	-34.60	40.88	-56.83	17.33	133.66	3125	3125	0.565
55	0.8	0.15	138	0.25	81.74	90.22	73.09	1.89	133.78	139.31	128.13	1.37	-16.39	-5.02	-28.12	5.08	157.63	9375	9375	0.854
56	0.8	0.15	138	0.25	80.76	90.10	72.32	1.88	131.60	136.53	126.34	1.28	-16.23	-4.55	-26.89	4.83	155.25	9375	9375	0.902
57	0.8	0.15	200	0.15	65.17	73.94	57.81	1.88	97.11	104.31	89.67	1.96	-11.55	-2.27	-20.85	4.27	117.52	3125	3125	0.711
58	0.8	0.15	200	0.15	62.87	71.32	55.62	1.76	92.69	100.49	85.99	1.94	-17.47	-10.84	-24.15	2.73	113.35	9375	9375	0.600
59	0.8	0.2	107	0.1	57.01	118.66	-35.10	4.27	99.76	174.81	73.95	5.41	-22.23	33.87	-46.99	14.22	117.03	9375	9375	0.385
60	0.8	0.2	107	0.1	58.00	72.90	44.56	2.35	92.47	104.29	85.43	2.02	-54.09	-36.53	-71.44	8.44	121.82	3125	3125	0.461
61	0.8	0.2	107	0.2	80.93	94.11	94.11	2.50	135.92	141.84	128.63	1.44	17.35	42.85	-6.75	12.44	159.14	9375	9375	1.259
62	0.8	0.2	107	0.2	81.82	94.04	71.52	2.47	141.14	148.46	133.72	1.67	25.70	45.48	6.56	9.28	165.15	9375	9375	0.693
63	0.8	0.2	169	0.2	86.32	96.63	75.34	2.20	139.36	147.34	131.26	1.95	14.27	26.30	3.09	4.83	164.55	3125	3125	0.445
64	0.8	0.2	169	0.2	82.17	94.78	94.78	2.94	136.27	136.27	125.52	2.88	-26.09	-13.74	-38.48	4.81	161.25	3125	3125	0.466
65	0.8	0.2	169	0.1	67.49	120.63	13.26	3.64	90.99	159.87	70.17	4.60	5.34	39.61	-12.22	8.21	113.41	3125	3125	0.540
66	0.8	0.2	169	0.1	67.55	81.71	58.68	2.45	89.63	98.76	83.08	2.01	12.98	26.83	0.60	5.85	112.98	3125	3125	0.372
67	0.8	0.25	138	0.15	78.03	137.61	19.05	4.21	136.51	186.05	118.29	4.50	-42.20	-15.38	-62.96	6.13	162.80	3125	9375	0.367
68	0.8	0.25	138	0.15	70.23	79.17	61.15	1.99	115.06	121.22	108.68	1.48	21.92	40.01	3.47	8.72	136.57	3125	3125	0.535

where k_c is the specific cutting constant (in N/mm^2) and *A* is the cutting cross-section. They can also be observed in the theoretical surface roughness model shown in Figure 9, in which *Z* is the peak-to-valley distance, and a_r is to the cutting depth recommended by the tool provider (shown for comparison). Note that Equations (5) and (6), as well as the models in Figure 9, have all been widely used in previous work[4,21,22].

Both the models in Figure 9 and results given by Equations (5) and (6) agree with the results of the correlation analysis conducted in this study: *a* and *f* exhibited strong correlations with *AvgFc* because high values for these parameters result in a higher *A*, increasing *Fc*. Furthermore, *f* and*r*respectively exhibited positive and negative correlations with *Ra*. The theoretical models illustrated in Figure 9 demonstrate the effects of these two parameters on *Z*, which significantly influences *Ra*. Note that the complex interactions between the tool and workpiece, as well as chip breakage, material defects, and other uncertainties will inevitably result in minor deviations from the models shown in the figure[21,23]. Finally, although the applied *υ* directly affects the scale of the horizontal surface profile, this change only slightly influences *Ra*, explaining the low correlation between these two features.

Notably, although the analysis results indicated that a smaller *a* yielded a higher *Ra*, this has not typically been observed during general turning processes. This unconventional trend may be caused by the low range of *a*considered in the dataset (0.05–0.25 mm) compared with the *a* values applied in typical turning operations or even the a_r values recommended by tool provider (1 and 1.5 mm in Table 4)[3,9,10]. This can be observed in Figure 9, which shows that small cutting depths cause the tool to only "scratch" the workpiece surface without fully engaging it, such that little cutting actually occurs; these size effects have been reported to correlate with reduced cutting stability[4,21]. Note that these relatively shallow *a* values are only used to achieve close tolerance and tight *Ra* requirements during high-accuracy turning operations, while avoiding workpiece undersizing that can lead

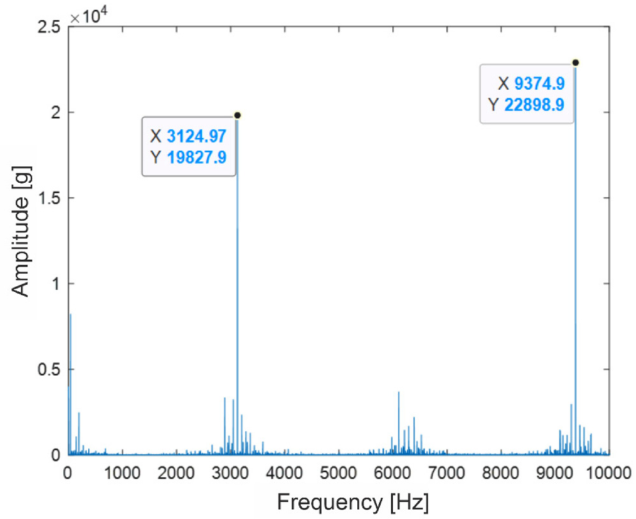

Figure 4. Frequency domain of the segmented acceleration signal

to workpiece rejection [23]. It is also known that v scales the surface profile horizontally such that it might give only slight changes to the *Ra* value. That is the reason for the low correlation value between v and Ra.

The results of the Pearson and Spearman rank correlation analyses were complemented by evaluations of the R^2 and p—values for the relationships between features, as shown in Figures 10 and 11, respectively. The R^2 values reflect the variance in the dependent variable (i.e., *Ra* or *AvgFc*) when predicted using the independent variable (i.e., each of the remaining features). Note that the R^2 analysis was based only on the Pearson correlation because R^2 is only applicable to linear relationships. The p—values reflect the statistical significance of the observed correlations, with a lower p—value indicating that the correlation is unlikely to occur by random chance.

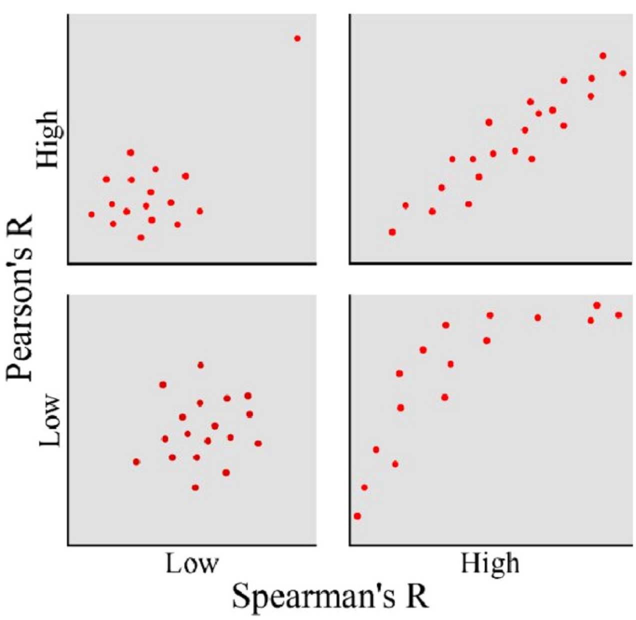

Figure 5. Relationships between two features based on Pearson and Spearman rank correlation [16]

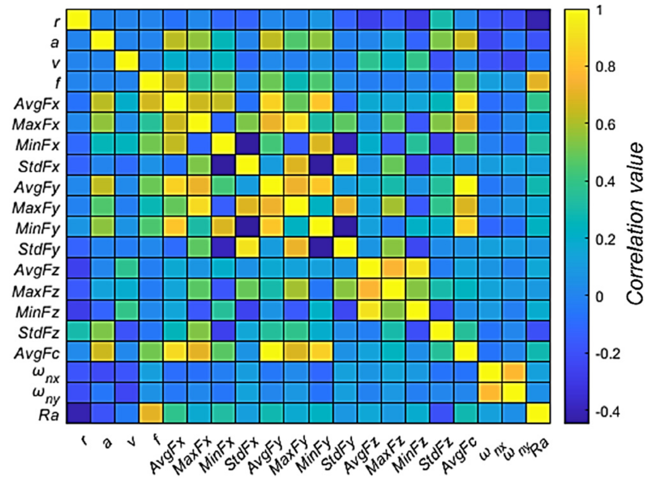

Figure 6. Pearson correlations among all features and Ra

Figure 10 indicates that the correlation between f and *Ra* exhibited the highest R^2 value of only approximately 0.5. However, relying solely on f to predict *Ra* will be insufficient, and the addition of other features, such as r and *AvgFc,* to *Ra* prediction models is recommended accordingly. Furthermore, the correlations between the various features and *AvgFc,* which is calculated by combining the average cutting forces in all directions, indicate that a and f exhibited relatively higher R^2 values than the other features. Therefore, f, r, a, and *AvgFc* were determined to exert the most influence on *Ra*. Indeed, Figure 11 shows that these four features are within the ideal p-value limit of 0.05, whereas the remaining features exhibit p-values above this limit for correlations with either *Ra* or *AvgFc.* Furthermore, note that features such as the *Max*, *Min*, and *Std* values of the forces in each direction were not reliable because the analysis indicated that they likely exhibited randomness during the turning process, affecting the integrity of their correlations with *Ra* and *AvgFc.*

These insights into the features exerting the greatest influence on *Ra* can inform efforts to increase the efficiency of turning process monitoring and data storage, which are critical concerns in the pursuit of intelligent machining [24]. Indeed, predictive models constructed to consider only a few highly correlated features can achieve superior performance and efficiency over models that

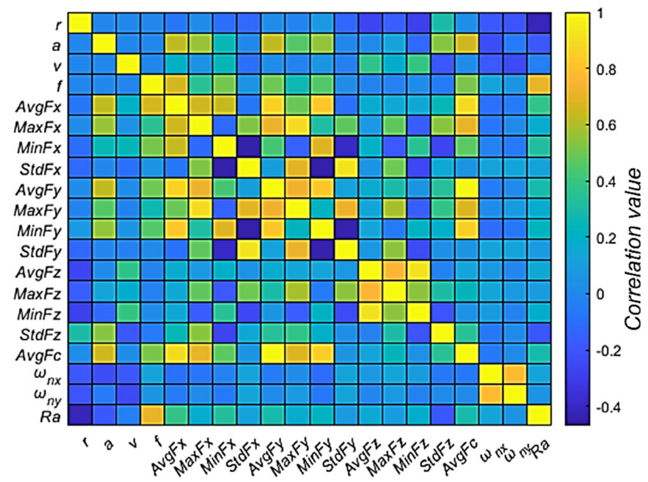

Figure 7. Spearman correlations among all features and Ra

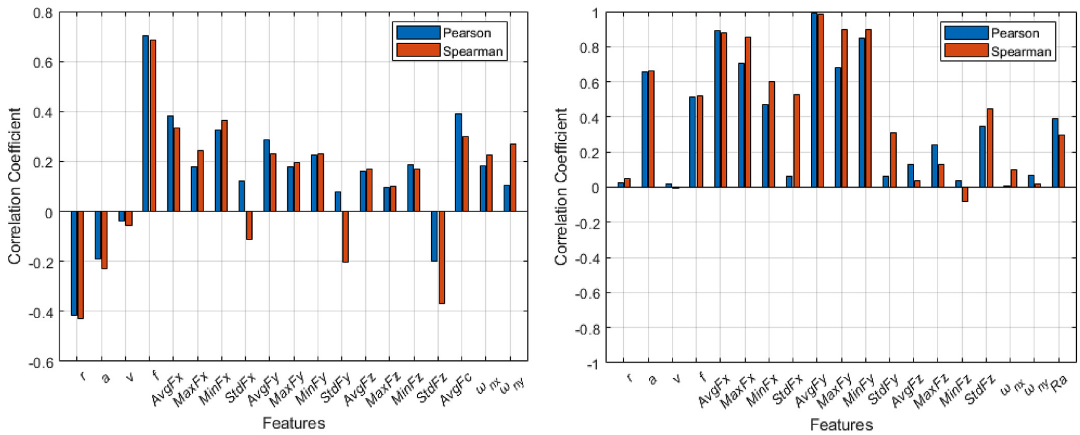

(a) *Ra* (b) *AvgFc*

Figure 8. Pearson and Spearman rank correlations between all features and (a) Ra and (b) AvgFc

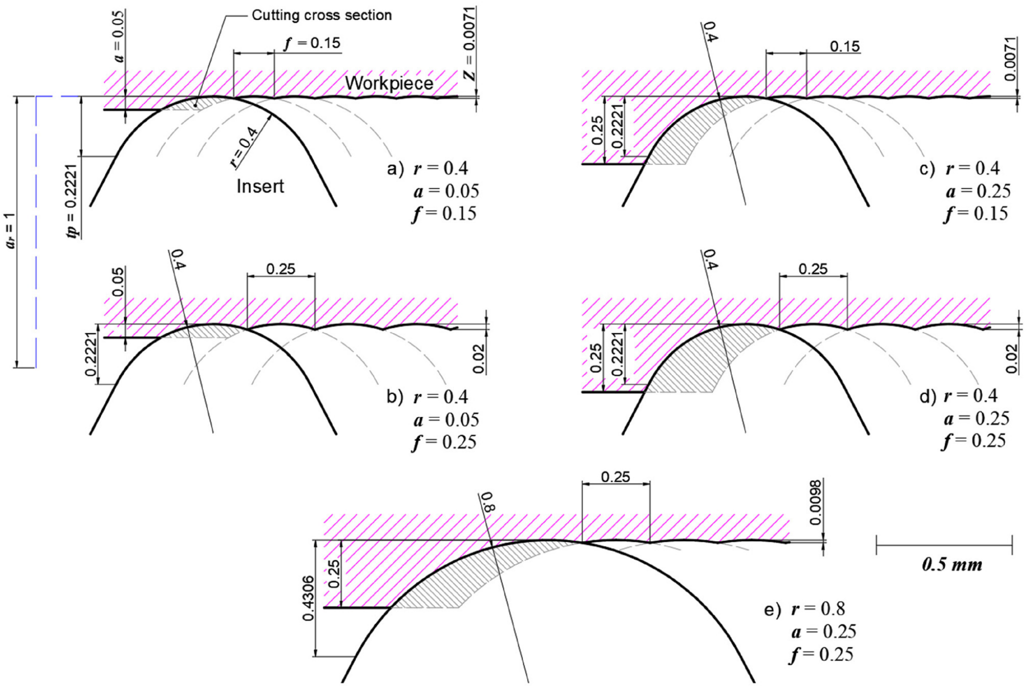

Figure 9. *Theoretical surface roughness models for various combinations of cutting parameters (units in mm)*

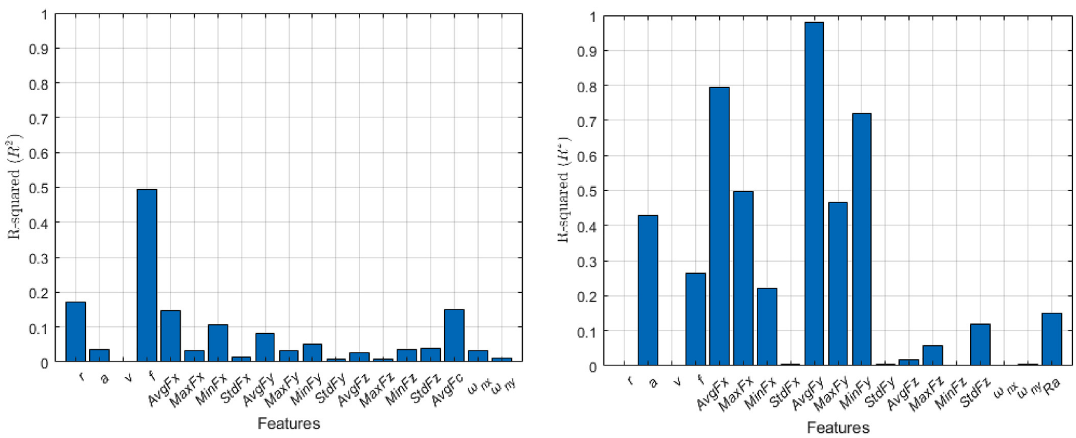

(a) *Ra* (b) *AvgFc*

Figure 10. R^2 values for the correlations between each feature and (a) Ra and (b) AvgFc

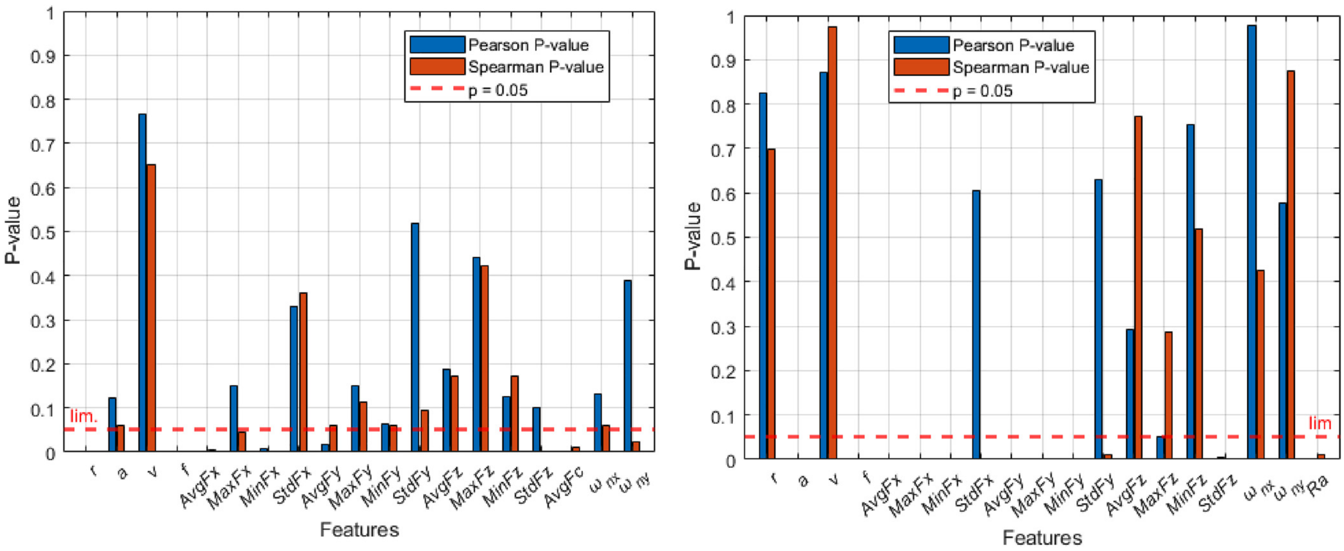

(a) *Ra* (b) *AvgFc*

Figure 11. p-values for the correlations between each feature and (a) Ra and (b) AvgFc

attempt to consider all measured data. Furthermore, the size of the dataset used for prediction can be significantly reduced by storing only relevant features.

5. CONCLUSIONS

This study proposed a method for processing signals and extracting relevant features from turning process data to inform a subsequent correlation analysis. First, Savitzky–Golay filtering was performed on the raw signals, then signal segmentation was undertaken to eliminate irrelevant information corresponding to roughing operations and noise from non-cutting movements while excluding outlier peaks originating from the initiation and breaking of tool contact. The mean, maximum, minimum, and standard deviation values of the segmented cutting force signals were subsequently obtained as features. The same process was applied to segment the corresponding acceleration signals are also segmented. The FFT was applied to obtain the signals in the frequency domain and determine the natural frequencies corresponding to the largest amplitude vibrations in the x- and y-directions. Finally, Pearson and Spearman rank correlation analyses were performed to determine the process parameter, cutting force, and vibration features most influencing the surface roughness *Ra*. Several features were determined to exert critical influences on *Ra*: the feed (f), corner radius (r), depth of cut (a), and average multidirectional cutting force (*AvgFc*). Among these features, only *AvgFc* directly characterized the current state of the turning operation, although all of these features give relatively high R^2 values for correlation with either *Ra* or *AvgFc*, and the p-values for the correlations between these features and either *Ra* or *AvgFc* were within 0.05. These results indicate that only f, r, a, and *AvgFc* need to be considered to predict the value of *Ra* with relatively high accuracy. Therefore, this study provides valuable insights for researchers and engineers constructing models for predicting *Ra* during turning operations, especially when conducting high-accuracy turning of high-strength 42CrMo4+QT workpieces. Table 8 presented in this study provides a convenient training or testing dataset when considering the recommended features as model inputs. Finally, the insights obtained by this study provide a useful basis for determining efficient data storage and management strategies for intelligent machining applications.

AFFILIATIONS AND AUTHOR DETAILS

Undergraduate Author

Farah Mohammed Fallata – *Mechanical Engineering Department, King Fahd University of Petroleum & Minerals, Dhahran 31261, Saudi Arabia;* 0009-0001-0611-6624
Email: s202253940@kfupm.edu.sa

Corresponding Authors

Muhammad Fadhlan Afif – *Graduate Author (PhD student), Mechanical Engineering Department, King Fahd University of Petroleum & Minerals, Dhahran 31261, Saudi Arabia;* 0009-0001-9807-546X
Email: g202304230@kfupm.edu.sa

Ahmed Aly Diaa Sarhan – *Research Mentor, Mechanical Engineering Department and Interdisciplinary Research Centre for Intelligent Manufacturing & Robotics, King Fahd University of Petroleum and Minerals, Dhahran 31261, Saudi Arabia;* 0000-0001-8474-8347
Email: ahsarhan@kfupm.edu.sa;

ACKNOWLEDGEMENTS

The authors thank the King Fahd University of Petroleum and Minerals and the Interdisciplinary Research Center for Intelligent Manufacturing and Robotics for providing financial and technical support. This work was funded by the KFUPM-IM & R-Funded Grant Project Code: INMR2407.

REFERENCES

(1) Pramanik, A. *et al.* Fatigue life of machined components. *Adv Manuf* **5**, 59–76 (2017).

(2) Cui, T. *Precision Machining of Hard-to-Cut Materials: Current Status and Future Directions. IJACSA) International Journal of Advanced Computer Science and Applications* vol. 15 www.ijacsa.thesai.org (2024).

(3) Díaz-Salamanca, D. *et al.* Turning of 42CrMo4+QT under different scenarios: Dataset of machining, roughness and residual stress. *Data Brief* **56**, (2024).

(4) Díaz-Salamanca, D. *et al.* Influence of turning parameters on residual stresses and roughness of 42CrMo4 + QT. *International Journal of Advanced Manufacturing Technology* **134**, 2897–2919 (2024).

(5) Diego, D.-S. *et al.* Assessing the Influence of Surface Roughness and Residual Stresses on the Fatigue Behaviour of 42CRMO4+QT Steel. in *Book of Abstracts of the 3rd International Symposium on Risk Analysis and Safety of Complex Structures* (2025).

(6) VII. Note on regression and inheritance in the case of two parents. *Proceedings of the Royal Society of London* **58**, 240–242 (1895).

(7) N F H, M. Pearson Correlation Analysis between Radius and Surface Roughness (Ra) Measurements during Turning Processes. *International Journal of Advanced Trends in Computer Science and Engineering* **9**, 237–241 (2020).

(8) Swiss Steel Group. *Technical Datasheet 42CrMo(S)4 +QT +SH.* www.swissgreensteel.com (2023).

(9) SANDVIK Coromant. DCMX 11 T3 04-WF 4325 CoroTurn®107, insert for turning. *Product details* (2025).

(10) SANDVIK Coromant. DCMX 11 T3 08-WF 4425 CoroTurn®107, insert for turning. *Product Details* (2025).

(11) Walter, G. & Jaroslav, B. *Solving Problems in Scientific Computing Using Maple and Matlab*. (Springer Verlag, 2004).

(12) Schafer, R. What Is a Savitzky-Golay Filter? *IEEE Signal Process Mag* **28**, 111–117 (2011).

(13) Frigo, M. & Johnson, S. G. FFTW: An Adaptive Software Architecture for the FFT. in *Proceedings of the International Conference on Acoustics, Speech, and Signal Processing* 1381–1384 (1998).

(14) MATLAB. fft Documentation. *MATLAB Help Center* (2025).

(15) Bistacchi, A., Mittempergher, S., Martinelli, M. & Storti, F. On a new robust workflow for the statistical and spatial analysis of fracture data collected with scanlines (or the importance of stationarity). Preprint at https://doi.org/10.5194/se-2020-83 (2020).

(16) Zar, J. H. Spearman Rank Correlation. in *Encyclopedia of Biostatistics* (Wiley, 2005). doi:10.1002/0470011815.b2a15150.

(17) Feng, C., Li, M., Guo, H., Qiu, B. & Zhang, J. Energy efficiency identification and surface roughness prediction using cutting force signal for computer numerical controlled machine systems. *Sci Rep* **14**, 19004 (2024).

(18) Trinh, V.-L. A Review of the Surface Roughness Prediction Methods in Finishing Machining. *Engineering, Technology & Applied Science Research* **14**, 15297–15304 (2024).

(19) Khlifi, H., Abdellaoui, L. & Bouzid Saï, W. Prediction of Cutting Force and Surface Roughness in Turning Using Machine Learning. in 213–222 (2024). doi:10.1007/978-3-031-42659-9_24.

(20) Pasic, M. *et al.* Prediction and Optimization of Surface Roughness and Cutting Forces in Turning Process Using ANN, SHAP Analysis, and Hybrid MCDM Method. *Applied Sciences* **14**, 11386 (2024).

(21) Boothroyd, G. & Knight, W. A. *Fundamentals of Machining and Machine Tools Third Edition*.

(22) Horváth, R. & Lukács, J. Application of a force model adapted for the precise turning of various metallic materials. *Strojniski Vestnik/Journal of Mechanical Engineering* **63**, 489–500 (2017).

(23) Abellán-Nebot, J. V., Vila Pastor, C. & Siller, H. R. A Review of the Factors Influencing Surface Roughness in Machining and Their Impact on Sustainability. *Sustainability* **16**, 1917 (2024).

(24) Schaffer George H. ARTIFICIAL INTELLIGENCE: A TOOL FOR SMART MANUFACTURING. *American machinist & automated manufacturing* **130**, 83–94 (1986).